Franke, D., Neben, S., Schreckenberger, B., Schulze, A., Stiller, M., Krawczyk, C. M. (2006): Crustal structure across the Colorado Basin, offshore Argentina. - Geophysical Journal International, 165, 3, pp. 850—864.

DOI: http://doi.org/10.1111/j.1365-246X.2006.02907.x

Geophys. J. Int. (2006) **165,** 850–864 doi: 10.1111/j.1365-246X.2006.02907.x

Crustal structure across the Colorado Basin, offshore Argentina

Dieter Franke,[1] Soenke Neben,[1] Bernd Schreckenberger,[1] Albrecht Schulze,[2] Manfred Stiller[2] and Charlotte M. Krawczyk[2]

[1] *Fed. Inst. Geosciences & Nat Res. (BGR), Hannover, Germany. E-mail: Soenke.Neben@bgr.de*
[2] *GeoForschungsZentrum Potsdam, Germany*

Accepted 2006 January 10. Received 2005 December 12; in original form 2004 September 24

SUMMARY

The geology of the wide shelves surrounding the South Atlantic is closely linked to the kinematics and history of the opening of the ocean. However, several wide sedimentary basins, which developed along the margins show peculiarities that are not yet understood in the context of the evolution of the South Atlantic.

The Colorado Basin, a wide sedimentary basin on the broad shelf of Argentina, extends in EW direction. The basin's evolution oblique or orthogonal to the continent–ocean boundary indicates that it is not a product of simple progressive extension and crustal thinning. In addition a basement high, paralleling the continental margin and separating the Colorado Basin from the deep-sea basin is a common interpretation. These findings are hardly in accordance with the idea that the Colorado Basin is an extensional basin that developed in conjunction with the early E–W opening phase of the South Atlantic in the Late Jurassic/Early Cretaceous. The composition, type, and structure of the basement, key points for the evaluation of the basins evolution, are widely speculative.

In this context multichannel seismic reflection data from the Argentine Shelf and a 665-km-long onshore–offshore refraction profile, running across the Colorado Basin onto the coast are discussed in combination with gravity data. The stratigraphy for the sedimentary successions was adopted from the literature and the reflection seismic marker horizons formed besides the interval velocities the input for the starting model for refraction seismic traveltime modelling. The modelling strategy was an iterative procedure between refraction seismic traveltime and gravity modelling. The preparation of the density models was coarsely orientated on published velocity–density relations. The modelling results are in favour of a continuation of the main onshore geological features beneath the sedimentary infill of the Colorado Basin. We interpret the basement along the line from west to east as offshore continuation of the Ventana Hills, the Claromecó depocentre, and of Palaeozoic to Middle Mesozoic rocks of the Patagonia terrane. In the deepest part of the pre-/ synrift graben within the Colorado Basin a volcanic/igneous intrusion was interpreted forming an injection into an extensional fault.

According to our interpretation most of the Colorado Basin developed in conjunction with an early opening phase of the South Atlantic (150–130 Ma) and thus represents a typical rift basin instead of an intracontinental sag basin. The origin of the oblique rift most probably resulted from extensional stress, acting either through or interfering with the prevailing Palaeozoic basement fabric, oriented NW–SE. Although there was certainly a strike-slip component in the basins evolution and it may be interpreted as pull-apart basin we suggest that the Colorado Basin represents a failed rift structure: The basin's floor is more or less flat across the shelf, shows a slow rise at the shelf break and deepens towards the deep-sea basin where it finally merges with the seaward-dipping reflector sequences, and the basin probably was affected by magmatic/volcanic intrusives/extrusives associated with the opening of the South Atlantic.

Key words: Argentina, reflection seismology, refraction seismology, sedimentary basin, South Atlantic rifted margin.

INTRODUCTION

The Colorado Basin (Figs 1 and 2) is located on the broad shelf of the Argentine margin, having dimensions of 200 × 500 km (Bushnell *et al.* 2000). The basin complex is recognized as one of a series of aulacogenetic embayments whose axes are oriented transverse to the rifted continental margin. Other basins in this series include the Salado Basin and the Punta del Este subbasin that extend northwards along the Argentine and Uruguay shelf (Fig. 1). Three major depositional centres were identified within the Colorado Basin, of which the deepest is supposed to hold up to 15 km of sediment (Bushnell *et al.* 2000). The peculiarities of the Colorado Basin are:

(i) The Colorado Basin extends in EW-direction, that is, the basin is oblique or orthogonal to the continent–ocean boundary. That is surprising as it is commonly assumed that the final evolution of the basin took place in combination with a huge phase of extension in the Late Jurassic/Early Cretaceous, the early opening phase of the South Atlantic (Nürnberg & Müller 1991). The opening of the South Atlantic is predominantly characterized by an EW divergence of the African and South American plates (Nürnberg & Müller 1991) that is supposed to reflect in NS-trending rift basins with EW-dipping basin bounding faults.

(ii) A basement high, paralleling the continental margin and separating the Colorado Basin from the Argentine Basin (inlet in Fig. 1) is a common interpretation (Ludwig *et al.* 1979; Dingle *et al.* 1983; Maslanyj *et al.* 1992; Max *et al.* 1999; Bushnell *et al.* 2000). These authors argue that the basin thus is not the product of simple progressive extension and crustal thinning.

(iii) The composition of the basement is widely speculative. Information on the basement structures and lithology is a key point for the evaluation of the basin's evolution.

To contribute to the discussion of basin evolution this paper presents new multichannel reflection seismic (MCS) and refraction seismic data and a model of the Colorado Basin resulting from

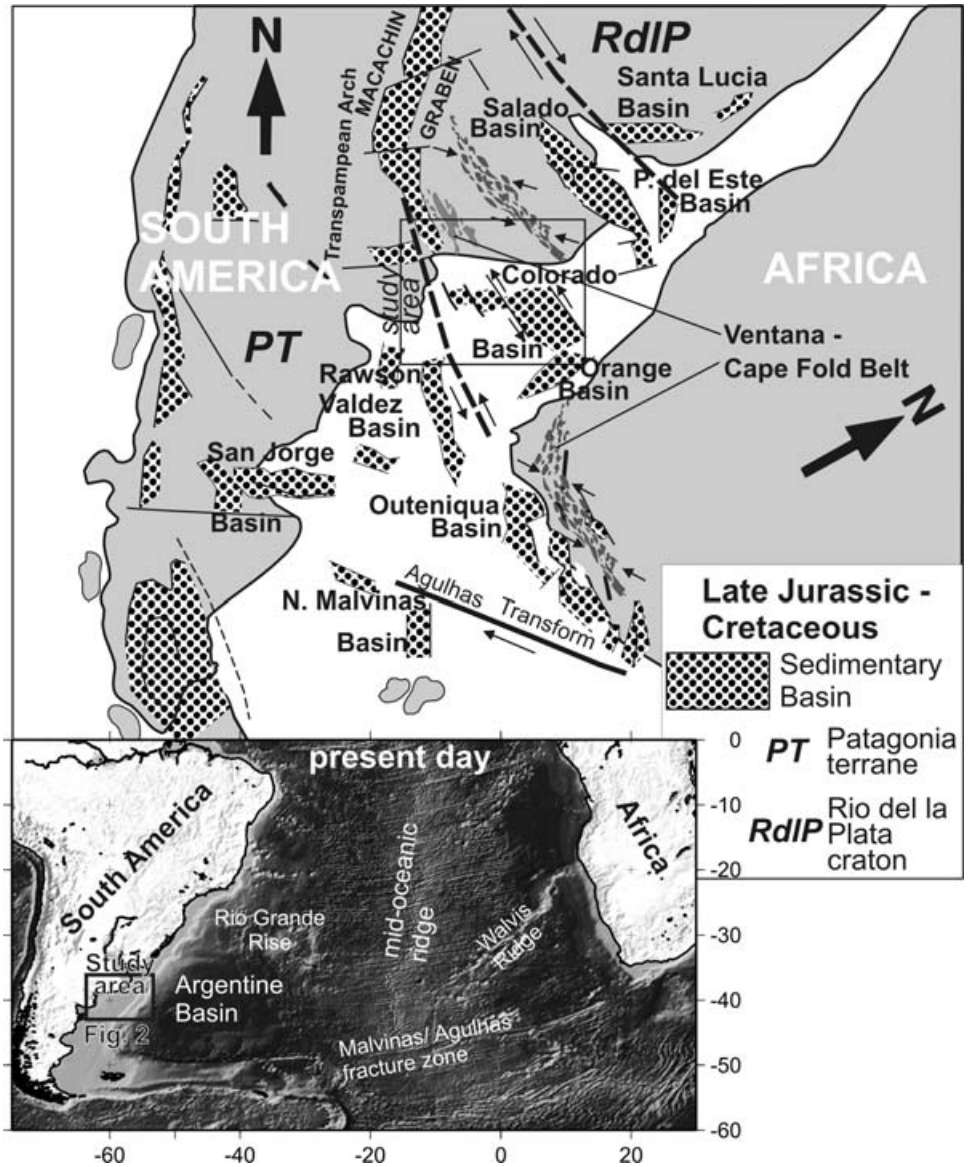

Figure 1. Late Jurassic–Cretaceous reconstruction of the South Atlantic (modified from Tankard *et al.* 1995). The supposed distribution of sedimentary basins initiated at that time is indicated. The inlet shows the present-day situation with the study area indicated.

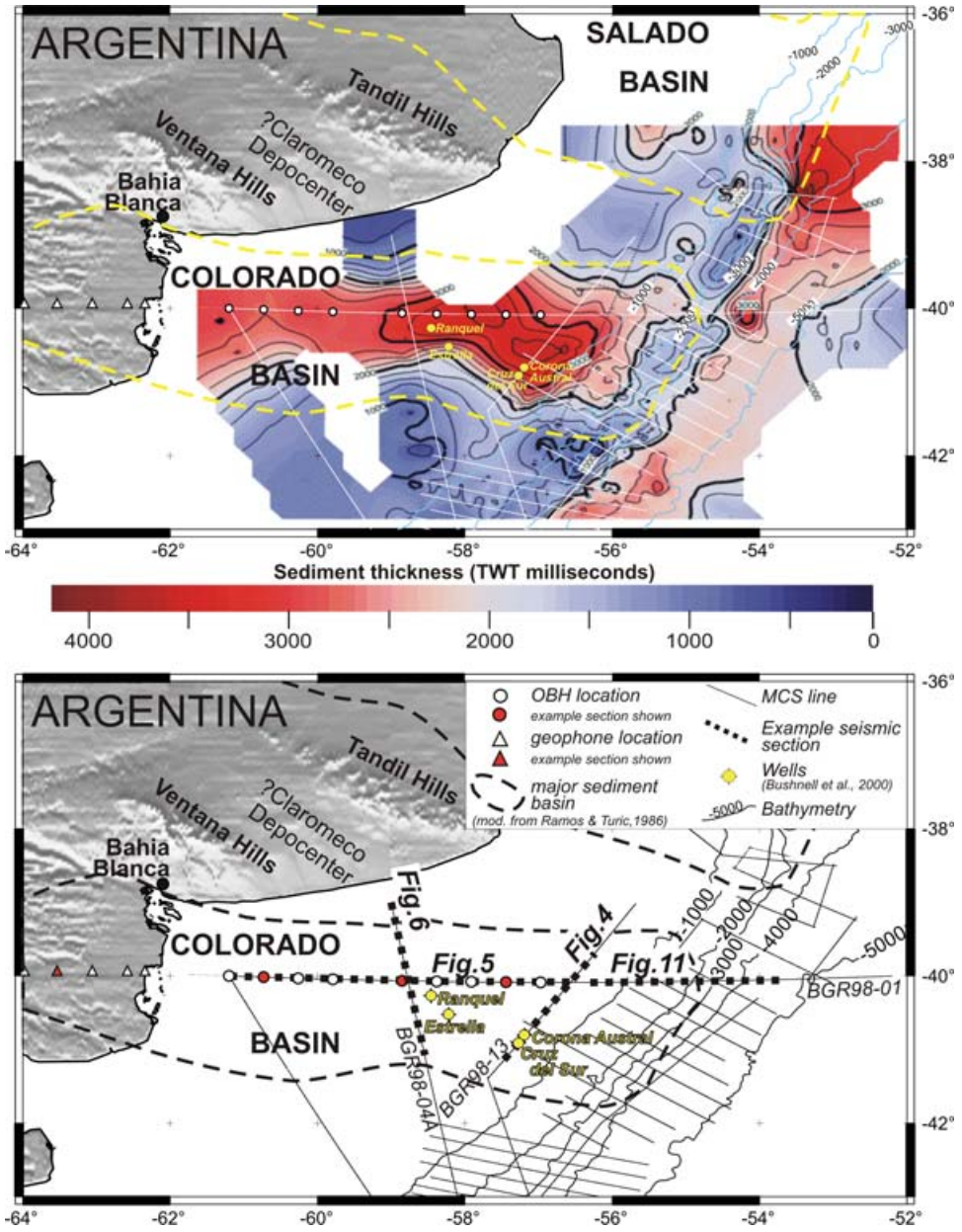

Figure 2. Thickness of sediments (seabottom minus BU) in milliseconds (two-way traveltime). Locations of the seismic lines illustrated and discussed in the text and the locations of the ocean bottom hydrophone (OBH) and geophone stations are indicated. The onshore limits of the Colorado and Salado Basins are from Ramos & Turic (1996).

gravity and refraction traveltime modelling. The seismic and gravity data were acquired by the Federal Institute for Geosciences and Natural Resources (BGR, Hannover, Germany) and the GeoForschungsZentrum (GFZ, Potsdam, Germany).

GEOLOGICAL FRAMEWORK

Basin evolution

The Colorado Basin exhibits a complex history that makes it difficult to examine an onset of rifting that resulted in the final formation of the basin (Tankard *et al.* 1995). Following the Palaeozoic dominantly compressional setting, rifting began in the Early Jurassic along the southern margin of Africa and progressed southwestwards in Patagonia (Urien *et al.* 1981). Within this first phase of extension the San Jorge Basin (Fig. 1) was formed in a backarc environment and the basin became restricted in the mid-Jurassic (Urien *et al.* 1981; Dalziel *et al.* 1987). Probably the Colorado Basin region was affected by this extension phase as well.

In Late Jurassic–Cretaceous, immediately before and during break-up of the South Atlantic, extension propagated inboard and was widely distributed (Uliana *et al.* 1989). A linked system of NW–SE orientated basins, associated with a northwest-trending dextral shear system (Tankard *et al.* 1995; *cf.* Fig. 1) developed along the shelf, including the Colorado Basin (Kelley & Light 1993; Urien *et al.* 1995). Whether this stage was a renewed period of rifting or a continuation of Triassic/Jurassic extension is still a matter of debate (Light *et al.* 1993). The final opening of the South Atlantic took

place in Early Cretaceous time (e.g. Rabinowitz & LaBrecque 1979; Unternehr *et al.* 1988; Nürnberg & Müller 1991; Lawver *et al.* 1998) with inferred opening ages for Argentina/South Africa ranging from 127.7 to 135.5 Ma. Most plate tectonic reconstructions describe the opening as a combination of complex rift and strike-slip faults and a stepwise, northward-propagating rift for the South Atlantic.

Onshore geology and basement composition

The composition of the Colorado Basins basement is still under discussion. Especially the influence of volcanic material is not yet clear. During the Late Palaeozoic essentially no magmatic activity was recorded in this province (Uliana *et al.* 1989). Northeastern Argentina formed in this period an interior and comparatively stable piece of the Gondwana continent. Basement of this Gondwana area comprises localized high-grade Archean cores, isolated within mid Proterozoic and Late Proterozoic mobile-belt terranes (Tankard *et al.* 1982; Uliana *et al.* 1989). According to Kelley & Light (1993) the basement in the Colorado Basin area is formed by Pre-Cambrian igneous and metamorphic rocks that are exposed on the Uruguayan side of the Rio del la Plata as pelitic gneiss and in the Tandil Hills (Fig. 2) as granite and migmatite (Iniguez *et al.* 1989) or Permo–Carboniferous sedimentary rocks. These structures are assumed to be the result of accretionary processes and have been reactivated repeatedly (Light *et al.* 1993). Uliana *et al.* (1989) argue from the abundance of eruptive and volcanoclastic rocks in the onshore depositional sequences for the existence of widespread syn-extensional magmatism during the Middle/Late Triassic, with increasing activity during the Jurassic in the Colorado Basin. Urien *et al.* (1995) postulated that the entire Colorado Basin complex formed on a volcanic basement, similar to the Rawson-Valdez-Basin complex and the San Jorge Basin. Hinz *et al.* (1999) described the basement of the Colorado Basin as a series of imbricate thrust sheets or asymmetric folds characterized by strong reflectivity and seismic velocities of more than 5 km s^{-1}. The imbricate units were tentatively linked to the Ventana and Tandil Highs.

Between the Ventana Hills and Tandil Hills (Fig. 2) asymmetrical folded successions of diamictides, sandstones and dark shales the so-called Claromecó depocentre (or Ventana Basin) is anticipated (e.g. Tankard *et al.* 1995; Urien *et al.* 1995; Fryklund *et al.* 1996, Fig. 2). The interpretation of a basin at this location is predominantly derived from potential field data and it is assumed to have developed as backarc basin associated with the Gondwanide Ventana-Cape Fold Belt evolution (Light *et al.* 1993). The proposed Claromecó depocentre is supposed to be filled with weakly metamorphosed marine sediments (Urien *et al.* 1981). Juan *et al.* (1996) suggested that the offshore extension of the Claromecó depocentre is the pre-rift formation in the Colorado Basin marked by a section of subcropping Palaeozoic (Permian) clastics.

DATA ACQUISITION AND PROCESSING

In 1998, a 457-km-long wide-angle seismic reflection/refraction profile and MCS lines were shot along latitude 40°S (Fig. 2) across the Colorado Basin. In addition to nine ocean-bottom hydrophone (OBH; Flueh & Bialas 1996) systems, with a spacing of about 40 km, five three-component seismometers were operated in the western prolongation of the refraction seismic line REF1 (see Table 1). Thus the total refraction profile length is 665 km and covers nearly the entire Colorado Basin. The land stations used were Teledyne PDAS-100 six-channel digital recorders, each with a three-component geophone Mark L-4C-3D (1 Hz) and a six-geophones string Sensor SM-6 (4.5 Hz, p recorder). The data were recorded with a sample rate of 10 ms. The records of the absolute time were synchronized by GPS receivers. The stations were established as accurately as possible on the same great circle as the line REF1, through the points 40°S, 61°12′W and 40°S, 52°40′W. Station 1 was installed directly at the coast, the other stations with increasing distances westwards. All stations and all geophones were buried. The stations near to the coast show longer ranges than those more inland.

Table 1. List of the positions and elevations of the recording stations of refraction line BGR98-REF1.

Station no.	Latitude (S)	Longitude (W)	Elev./depth
OBH1-1	40°05.21350′	56°58.32317′	−100.6 m
OBH1-2	40°05.04550′	57°26.54500′	−97.5 m
OBH1-3	40°04.84367′	57°54.75300′	−96.4 m
OBH1-4	40°04.51500′	58°22.95050′	−90.8 m
OBH1-5	40°04.02533′	58°51.16933′	−85.6 m
OBH1-6	40°02.72400′	59°47.53150′	−60.8 m
OBH1-7	40°01.91833′	60°15.68683′	−52.4 m
OBH1-8	40°01.00200′	60°43.84000′	−46.8 m
OBH1-9	40°00.01817′	61°12.01633′	−31.8 m
Station 1	39°56.820′	62°19.580′	0 m
Station 2	39°56.550′	62°26.565′	1 m
Station 3	39°55.826′	62°46.566′	15 m
Station 4	39°54.185′	63°16.145′	30 m
Station 5	39°50.650′	64°08.560′	61 m
First shot	39°59.000′	61°45.000′	7.5 m
Last shot	40°05.000′	56°23.000′	7.5 m

The seismic source used for both the reflection and the wide-angle seismic data acquisition was a tuned set of four linear subarrays with 32 airguns between 0.62 L and 3.28 L volume (total 4258 in^3 resp. 69.8 L), deployed 7.5 ± 0.5 m below sea surface and fired at equidistant shot intervals at distances of 175 m (∼60 s shot time intervals at a speed of 5.4 knots). The positioning was by DGPS throughout the whole survey with presumably an absolute accuracy better than 10 m.

Shipboard gravity data were acquired along the refraction line BGR98-REF1 as well as on the coincident MCS line BGR98-01 using a LaCoste & Romberg air/sea gravimeter system.

Processing and data display of the seismic data was done with the FOCUS (release 4.1) software from CogniSeis, Houston, TX, USA. Wide-angle data processing included trace editing and minimum-phase bandpass filtering. Extensive tests with different f–k filters were done to minimize ground-roll amplitudes within the first seconds in the data. The water depth of less than 100 m along the profile probably caused these high amplitude breaks that show extensive spatial aliasing. For all recordings a predictive deconvolution with a design gate around the first break showing a velocity in the range of 6 km s^{-1} was applied. The first 2 s remained unchanged to keep the near offset reflection undisturbed. The seismic energy was sufficient to trace signals on the record sections to distances between 100 and 120 km, and data quality is good on average. The data are displayed with a reduction velocity of 6 km s^{-1}.

MCS lines discussed and shown in the following are BGR98-01, -01A, -01B, 01C, -04 and -13. For the MCS data acquisition the same source as for the OBH data acquisition was used and signals were received along a 4500-m-long digital SYNTRAK Type 480/16 streamer with a group length of 25 m. It consisted of 180 channels with 32 type T-4 hydrophones per channel and data were recorded up to 12 s two-way reflection time with a sample rate of 2 ms.

The shot distance was 50 m (∼18 s shot time intervals at a speed of 5.4 knots), resulting in a common midpoint (CMP) distance of 12.5 m and a fold of 45. After trace editing, true amplitude recovery and filtering a predictive deconvolution was applied. Stacking velocities were determined every 3 km (every 240th CMP gather, respectively). The analyses were done interactively using semblance plots and corrected CMP gathers for control. After NMO correction and muting the CMP gathers were stacked resulting in 45-fold zero-offset traces spaced 12.5 m. A post-stack Kirchhoff-time migration was achieved to complete the processing sequence.

The standard processing sequence of the gravity data included the cross-correlation procedure described in LaCoste (1973), an instrumental drift correction, the tie of the survey to an absolute gravity station in Buenos Aires and a tidal correction. From the comparison of the two coincident lines we estimate that the final low-pass filtered free-air gravity values have an accuracy of about 2.5 mGal.

SEDIMENTARY SUCCESSIONS

Summaries for the different stratigraphic units within the Colorado Basin are given in Kaasschieter (1963, 1965), Urien & Zambrano (1973), Lesta *et al.* (1978), Turic & Diaz (1987), Fryklund *et al.* (1996), Hinz *et al.* (1999) and Bushnell *et al.* (2000). A summary of the stratigraphic concept and the nomenclature used in this study is shown in Fig. 3.

To illustrate the seismic image of the sedimentary successions Fig. 4 shows an example seismic section from the central part of line BGR98-13 [Shotpoint (SP) 1050-4700]. An extensional depocentre is controlled by normal faults on both sides and is filled with a thick (∼2 s twt) succession of synrift sediments. Strong, parallel reflectors beneath the break-up unconformity (BU; Fig. 4) are supposed to be organic shales or anhydrites as suggested by Bushnell *et al.* (2000) for the Cruz del Sur well location (Fig. 2). The increasing thickness of the section between the BU and the Colorado discontinuity towards the centre illustrates the basin's sag phase. Less affected from sag was the succession between the Colorado discontinuity and the Pedro Luro discontinuity. The Cretaceous Colorado and Fortin Formations (Fig. 3) are dominated by coarse continental to shallow marine sandstones and conglomerates (Bushnell *et al.* 2000) but their lithologic content is highly variable (Kaasschieter, 1963), and the distinction of the two formations is difficult (Fryklund *et al.* 1996). The Pedro Luro Formation (Palaeocene; Fig. 3) is predominantly bathyal shales (Bushnell *et al.* 2000). Palaeocene basalts were encountered within the Pedro Luro FM in the Puelche X-1 well (Lesta *et al.* 1978). The Neogene horizon (N; Fig. 4), dipping towards the NE, reflects the passive margin—fluvial/deltaic stage.

Line BGR98-01 runs along latitude 40°S in E–W direction across the Colorado Basin into the deep oceanic Argentine Basin. The western part of this line (BGR98-01C; Fig. 5) was shot twice. First a reflection seismic line and then a refraction seismic profile were acquired. The resulting model boundaries from the refraction seismic traveltime modelling are shown in two-way reflection time (s) superimposed on the MCS data in Fig. 5. The boundaries in the sedimentary succession fit quite well the interpreted marker horizons. The basins sag has its maximum obviously at the deep depocentre in a distance range from 280 to 400 km (Fig. 5). The sedimentary succession beneath the Colorado discontinuity is the most affected series by sag. The succession between the Colorado and the Pedro Luro horizons shows a more or less parallel layering while the Neogene horizon is dipping from ∼150 ms in the west to ∼1000 ms in the east. Beneath the BU pre-/ and synrift sediments are predominantly present in the deep depocentre mentioned before.

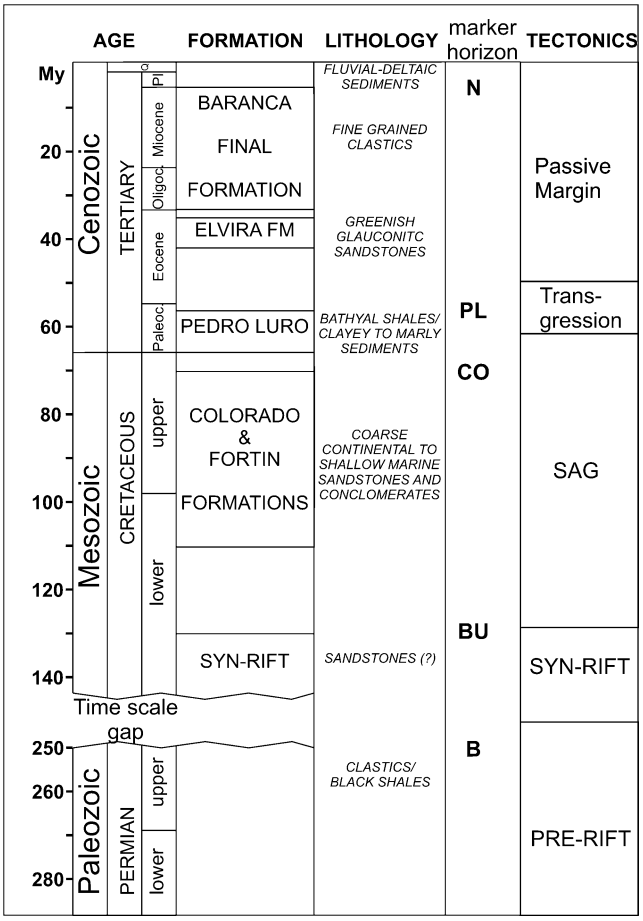

Figure 3. Generalized stratigraphy, lithology, seismic marker horizons and tectonic setting of the northern Argentine shelf adapted from Kaasschieter (1963, 1965), Urien & Zambrano (1973), Lesta *et al.* (1978), Turic & Diaz (1987), Fryklund *et al.* (1996), Hinz *et al.* (1999) and Bushnell *et al.* (2000).

The interpretation of faults affecting the basement is difficult. Only the eastern part of the deep depocentre (distance 350–400 km) is clearly affected by extensional faults resulting in the formation of a half-graben. It may be possible that extensional faults, which are related to the major Late Jurassic/Early Cretaceous extensional phase, are partly masked because the line direction is EW, that is, almost perpendicular to the proposed extensional forces affecting the basin. However, we suggest that the hummocky relief of the top of the basement is an expression of buried extensions of the Ventana and Tandil Highs (*cf.* Fig. 2). The inferred asymmetric faults that are shown in Fig. 5 (distance 200–320 km) are in accordance with the assumption of Late Palaeozoic compression resulting in the formation of the Ventana-Cape Fold-Belt (Light *et al.* 1993). Around a distance of 330 km the presence of magmatic intrusives/extrusives was interpreted in a region where the MCS data show low reflection amplitudes with no internal structuring. This is discussed in more detail in the chapter dealing with the refraction velocity-depth model. In that context it may be argued that the strong reflectors beneath the BU, in an offset range of 300–350 km may also represent basalts and pyroclastic rocks similar to the Palaeocene basalts

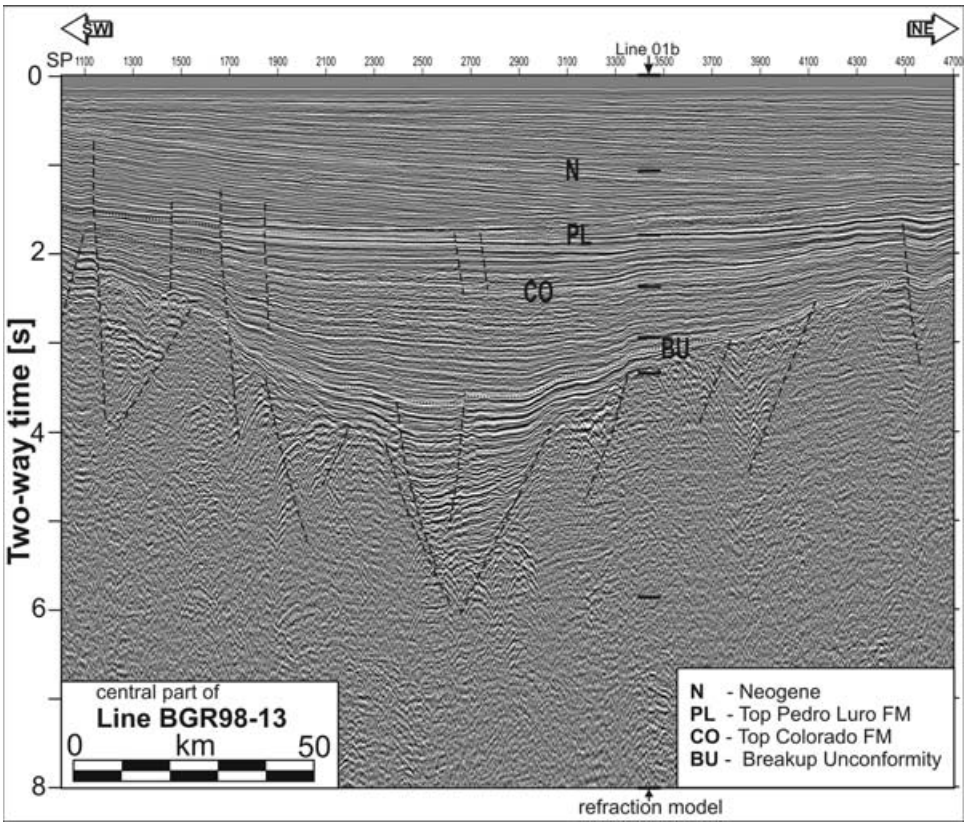

Figure 4. Interpreted seismic section from migrated line BGR98-13 showing the deepest part of the Colorado Basin. The data are displayed with an AGC (1000 ms). The seismic marker horizons (see Fig. 3) of the sedimentary sections discussed in the text are indicated. For location of the line see Fig. 2.

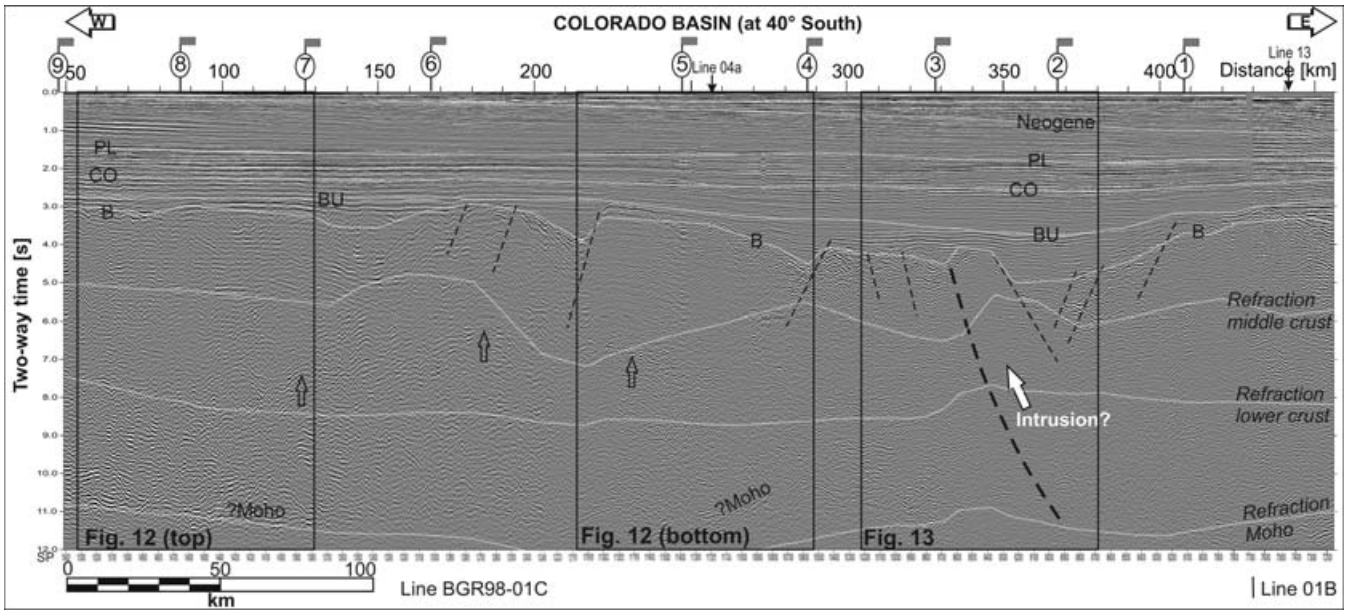

Figure 5. Reflection seismic line BGR98-01C running in EW direction across the Colorado Basin. The data are displayed with an AGC (1000 ms). Superimposed are the boundaries from the refraction seismic model converted to two-way traveltime. Nomenclature of the horizons as in Fig. 3. The open arrows mark locations of high reflective middle/lower crust in the MCS data and the larger white arrow indicates a zone of low reflectivity that is interpreted to result from an intrusion. For location of the line see Fig. 2. Cut-out sections shown in Figs 12 and 13 are indicated.

encountered in the Puelche X-1 well within the Pedro Luro FM (Lesta *et al.* 1978).

Line BGR98-04A (Fig. 6) is another profile running NS across the Colorado Basin. It shows a sedimentary succession with a maximum thickness of 3.5 s (twt) above the BU that is mainly controlled by sag. The syn-/ and pre-rift sequences below the BU are dissected by normal faults. The overall shape of the basin is best described as a half-graben with the major basin bounding faults in the north.

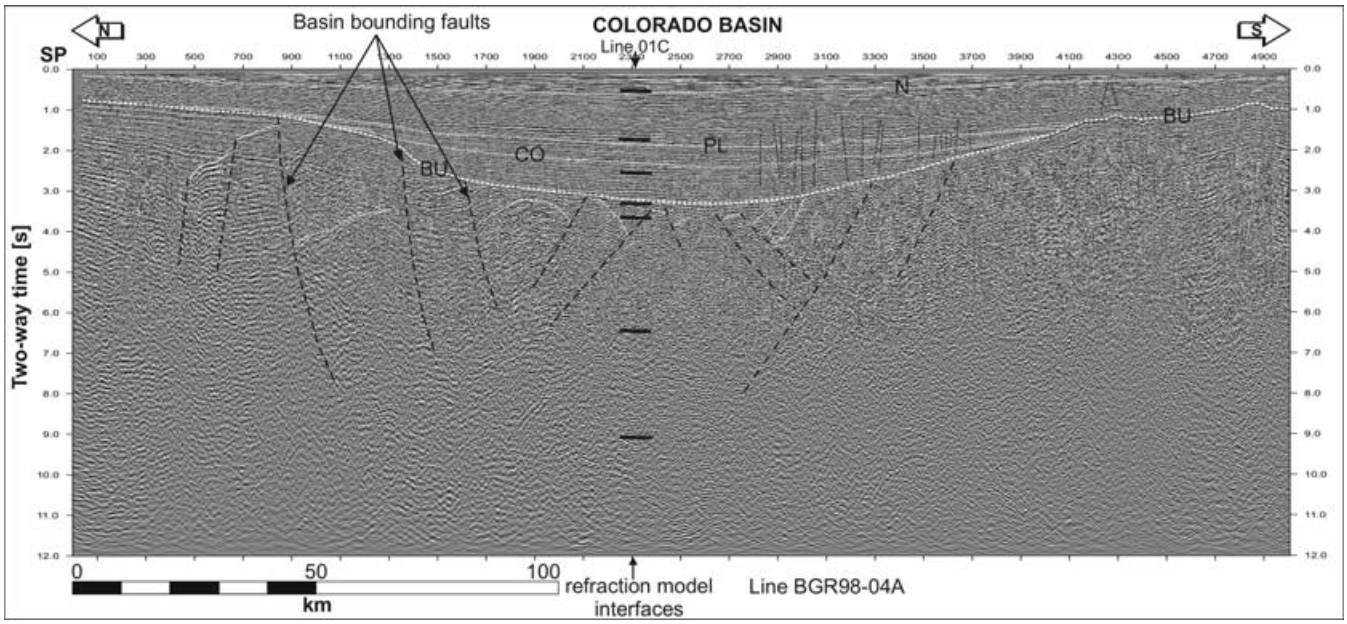

Figure 6. Reflection seismic section from migrated line BGR98-04A traversing the Colorado Basin in NNW–SSE direction at ∼58° 30′E. The data are displayed with an AGC (1000 ms). The seismic marker horizons are indicated (for the nomenclature see Fig. 3). The horizons from the refraction seismic model converted to two-way traveltime are shown at the cross-point location. For location of the line see Fig. 2.

REFRACTION AND GRAVITY MODELING

Primary *P* phases from refracted waves were identified in each receiver gather and their arrival times were interactively picked. The quality of the achieved velocity-depth model mostly depends on the qualitative estimate of phase identification. First arrivals of the OBH data in the near-offset range (<50 km) could be accurately identified with uncertainties less than ±50 ms. At larger offsets, accuracy step by step declines to about ±100 ms due to a lower signal-to-noise ratio.

Figs 7 and 8 illustrate refraction seismic data examples. The OBH station examples are displayed with a reduction velocity of 6 km s^{-1} and the *z*-component of the land station example with a reduction velocity of 8 km s^{-1}. Calculated traveltime picks are superimposed on the seismic sections. Four breaks from the sedimentary successions labelled Psed (*P*-wave velocities: 2.1, 2.3, 3.5, 4.25 km s^{-1}) are followed by a break that is labelled Pbu in the data examples. This break, with an average velocity of 4.8 km s^{-1} that increases to 5.2 km s^{-1} in the deep graben (distance 280–400 km; Fig. 9) correlates with the BU (compare Fig. 5) in the reflection seismic data. Pg is the break from headwaves that travelled along the basement with velocities ranging from 5.5 to 5.9 km s^{-1}. P* denotes the refracted wave from the lower crust. This break is less distinct in comparison with the other phases but in the data from OBH-5 (Fig. 7; left side in the lower panel) a clear reflection (rP*) in addition to the refracted wave P* is visible indicating an additional boundary at this level. The difference in the measured and calculated traveltimes of about 100 ms at an offset of ∼50 km for OBH-5 (Fig. 7; left side in the lower panel) shows the limits of the velocity model obtained. *Pn* and *PmP* indicate respectively refracted and reflected waves from the crust-mantle boundary. The *Pn* wave was clearly identified in the data from OBH-2 (Fig. 7; upper panel), OBH-5 (Fig. 7; left side in the lower panel), OBH-8 (Fig. 8; right side in the upper panel), and in the onshore data (LS4; Fig. 8, lower panel).

A semi-automatic picking using a phase tracker was applied to the data with manual corrections and a pick spacing of 10 traces. To calculate the crustal velocity-depth model a 2-D kinematic ray-tracing algorithm was used. The theoretical rays and their corresponding traveltimes were calculated for a laterally heterogeneous model and subsequently compared to the measured traveltimes of the primary *P* phases. In an iterative process the velocity-depth model was adjusted until the calculated travel times adequately fitted the observed data. As modelling strategy an 'across-and-down' approach was used (Zelt & Smith 1992). The known bathymetry and the traveltime to the acoustic basement from the reflection seismic data formed the minimum-parameter/minimum-structure starting model (Zelt 1999). The layer velocities for the starting model were adopted from the reflection seismics interval velocities. In comparison with the reflection seismic data (Fig. 5), more layers were added successively from top to bottom when the observed data made them necessary. When the data could not be fitted with this approach additional velocity points, that is, lateral inhomogenities in the velocity model were added. The resulting final refraction model is shown in Fig. 9.

2-D gravity modelling was performed for the offshore parts of the reflection and refraction seismic profiles. Shipboard free-air anomaly data were available for an approximately 800-km-long profile starting 23 km east of the coast. Structural constraints for the western part of the gravity model (Fig. 10) came from refraction seismic modelling (Fig. 9) and from MCS line BGR98-01C (Fig. 5). The eastern part the model is constrained by the depth-migrated MCS sections BGR98-01A and -01B (Fig. 11). Here, the crustal velocities and the depth values for the major interfaces are less confined than in the refraction model. The modelling strategy was an iterative procedure between seismic and gravity modelling. Every new velocity model was checked with a gravity model. For the preparation of the density models published velocity–density relations (Ludwig *et al.* 1970) were used. Remaining discrepancies between measured and modelled gravity led to additional refraction seismic modelling efforts and to alternative models. Fig. 10 shows

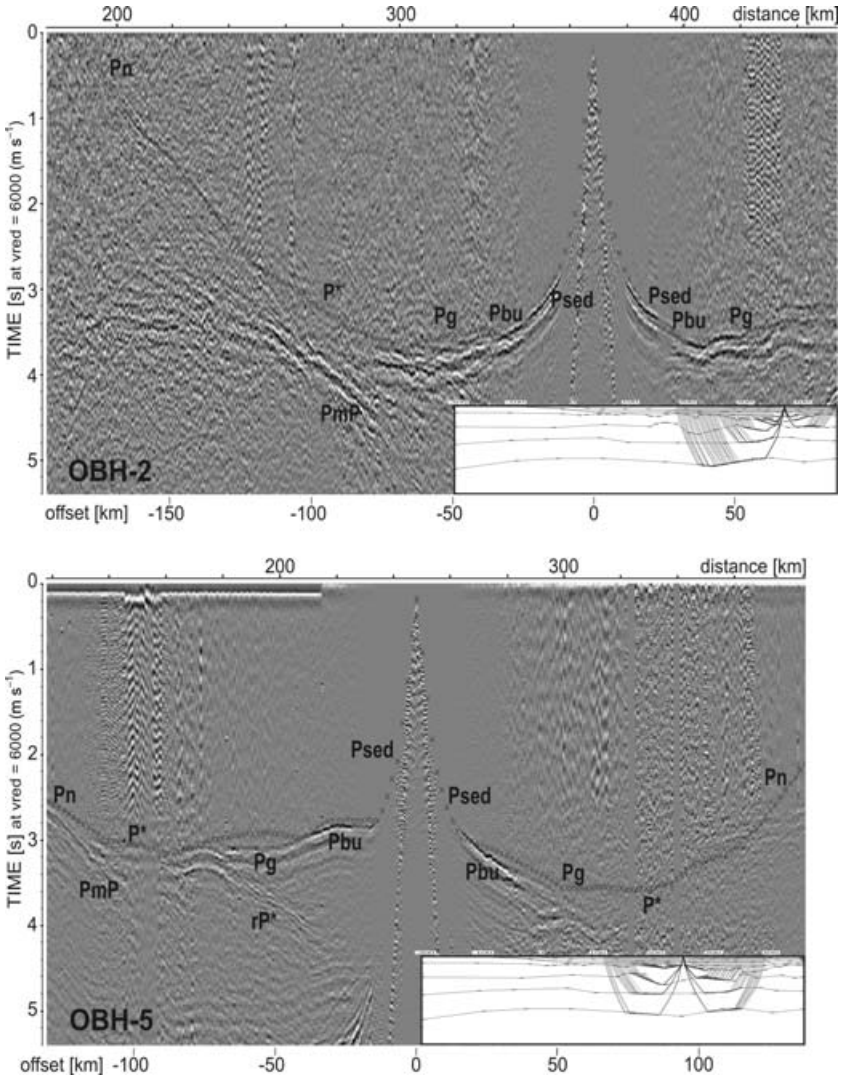

Figure 7. Refraction seismic data examples from the eastern end and the centre of line BGR98-01C (OBH2 & OBH5). The data are displayed with normalized amplitudes and a reduction velocity of 6 km s^{-1}. The distance shown on top of the data corresponds to the same label in Figs 5 and 9. Synthetic traveltimes, calculated for the velocity-depth model shown in Fig. 9, are superimposed and selected refracted phases are labelled. For location of the stations see Figs 2 and 5.

the final density model compared with the geometry of the final velocity model (Fig. 9). Most parts of the free-air gravity anomaly are reproduced by the calculated anomaly within a few mGal except of one part of the line (420–450 km) where we were unable to find a model that satisfies the gravimetric and seismic observations simultaneously. The major discrepancy between the results of the gravity model and the seismic data is the presence of a distinct minimum at 450 km between two gravity highs (Fig. 10). The maximum at 600 km is caused by a high-density body (2.9 g cm^{-3}) in the Middle crustal layer which we interpret as an intrusion while the other gravity high coincides with the shelf break. To fit the minimum between the highs we introduced a low-density body at a relatively shallow position. As indicated in Fig. 10 as an alternative we replaced a 30-km-wide part of the upper crust (2.7 g cm^{-3}) by a half-graben showing a lower density (2.55 g cm^{-3}) that would be more typical for sediments. Now our model fits the observed gravity data (stippled anomaly curve in Fig. 10) but indications for a deep sedimentary graben are missing in the reflection and refraction seismic data. As we have—at this position—a constraint on the 3-D structures from the nearby crossing line BGR98-13 we suggest that 3-D effects cause this gravity minimum. Some 20 km southwest of the cross-point of the two lines is the deepest part of the Colorado Basin (Fig. 4). It appears likely that the gravity minimum reflects this deep graben rather than a suspicious structure exactly in line direction. Another problem is an obvious misfit between the locations of the upper/middle crust boundary in the density and the velocity models at 150–200 km (Fig. 10). It was not possible to bring the refraction seismic data, showing a good coverage in this area, in accordance with the gravity data. We suspect that this difference is also caused by 3-D effects.

Modelling results

The refraction model extends from −200 km to a distance of 465 km and covers a depth of up to 40 km (Fig. 9). The first shotpoint from both the refraction profile and the coincident acquired reflection seismic line BGR98-01 corresponds to the distance 0 km. This location is approximately 23 km to the east of the shoreline.

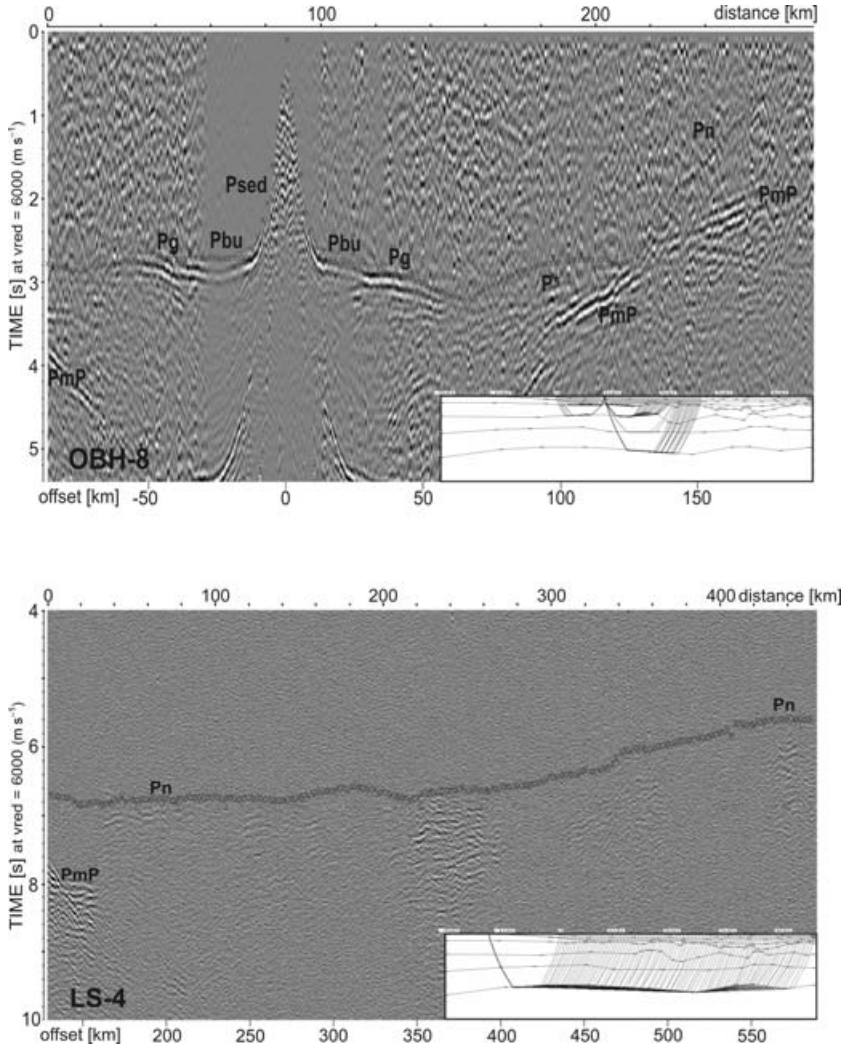

Figure 8. Refraction seismic data examples from the western end of line BGR98-01C (OBH8) and from an onshore geophone stations (LS4). The data are displayed with normalized amplitudes and a reduction velocity of 6 km s^{-1} (top) and of 8 km s^{-1} (bottom). The distance shown on top of the data corresponds to the same label in Figs 5 and 9. Synthetic traveltimes, calculated for the velocity-depth model shown in Fig. 9, are superimposed and selected refracted phases are labelled. Please note the Moho-arrivals in the lower panel that were recorded for distances of more than 550 km. For location of the stations see Figs 2 and 5.

The sedimentary succession down to the BU consists of four layers. The boundaries of these layers were derived from the interpretation of the reflection seismic data. In the marine area, that is, east of km 0, the close fit of the refraction boundaries with the marker horizons identified in the MCS data (line BGR98-01C) shows that the four main horizons also reflect velocity contrasts caused by, for example, lithological/depositional changes. Besides a small velocity increase towards the basins maximum sedimentary infill at a distance of 350 km, which may be explained by the increase of the sedimentary load, for the uppermost four layers no gradients were necessary to obtain a reasonable fit of the data. The velocities of the individual layers increase from top to bottom from 2.1, 2.3, 3.5 to 4.25 km s^{-1}. These sections comprise the Neogene infill plus the Pedro Luro and the Colorado/Fortin Formations. In the gravity model these sediments were modelled with two layers showing densities of 2.20 and 2.45 g cm^{-3}, respectively (Fig. 10). A layer with a velocity of 4.8–5.2 km s^{-1} and a density of 2.55 g cm^{-3} is present beneath the BU and is interpreted to represent Lower Cretaceous or even older synrift sediments. The highest velocities are present in the deepest part of the basin (km 280–410) possibly indicating the presence of magmatic intrusives/extrusives. In landward direction, that is, west of km 0, only the bottom of the sedimentary layers was recorded by land stations 1 and 2. The decrease of the thickness of the sediments towards the west is, therefore, speculative and mainly based on the proposed onshore projection of the Colorado Basin as shown by, for example, Urien & Zambrano (1996).

The basement section is heterogeneous along the profile. This is documented in the MCS data (Fig. 5) and confirmed by the wide-angle data (Fig. 9). Again the westernmost part of the line, that is, the distance from −205 to 0 km is only rarely covered by rays and, therefore, speculative. However, the distance range 0–400 km is well covered by rays and the modelled basement layer follows a distinct reflection pattern in the MCS data and may, therefore, be considered as well constrained. Around the distance at 0 km the smooth basement shows a relatively low velocity of 5.5 km s^{-1} that increases to 5.7–5.9 km s^{-1} between 50 and 270 km distance and shows a more pronounced relief that is confirmed by the reflection seismic data. The basement is dissected by numerous faults resulting

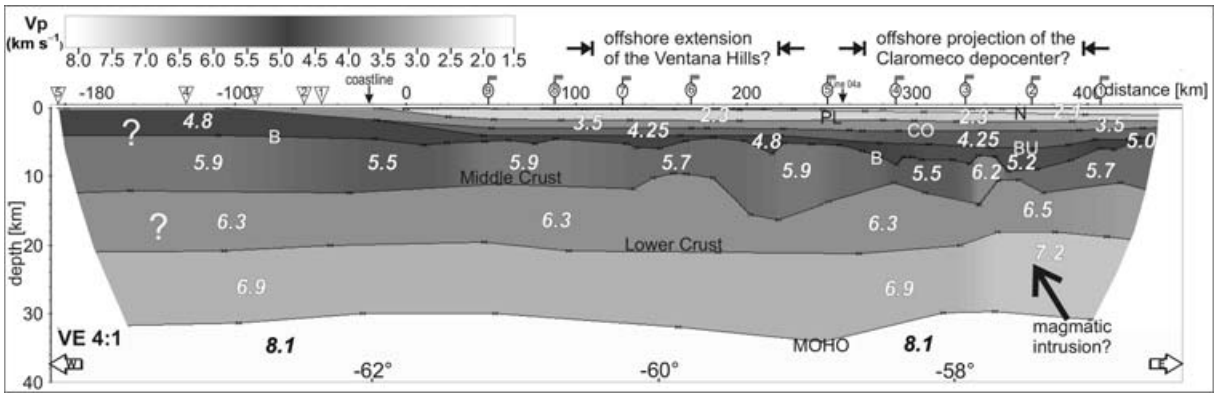

Figure 9. Velocity-depth model for the Colorado Basin derived from the refraction seismic traveltime modelling. The numbers indicate *P*-wave velocities in km s^{-1}. The locations of the deeply buried offshore extension of the Ventana Hills, the Claromecó depocentre and of the proposed magmatic/volcanic intrusives/extrusives are indicated (see text). The nomenclature of the sedimentary layers is as in Fig. 3.

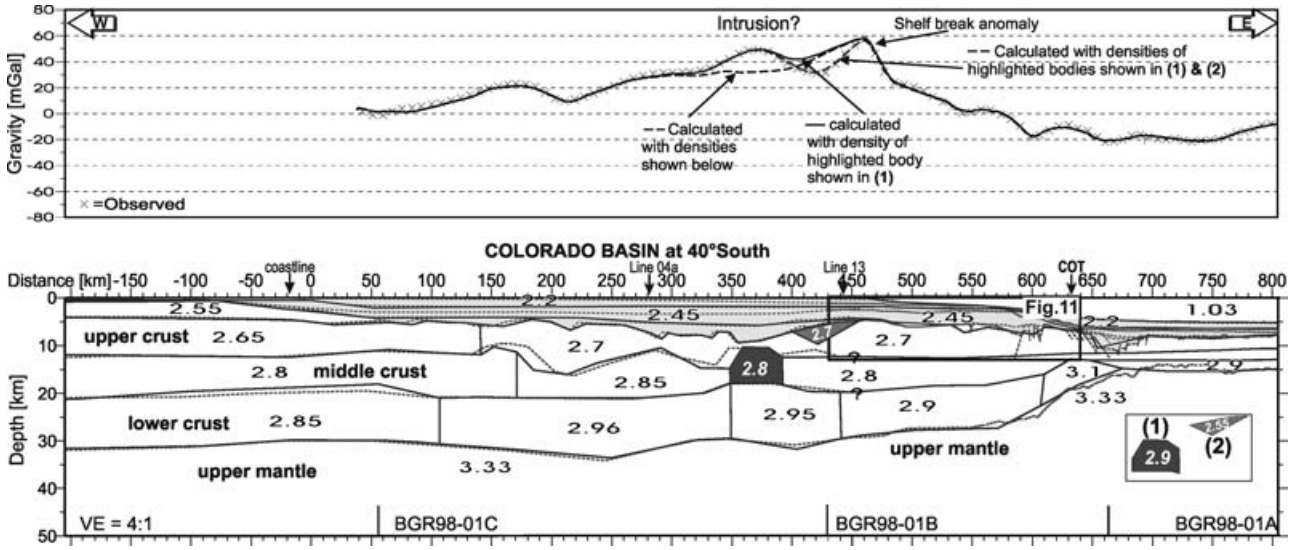

Figure 10. Gravity model for the combined seismic transect through the Colorado Basin. In the lower panel the density model (continuous lines) and associated density values in g cm^{-3} are shown. Light grey shading denotes sedimentary successions. For comparison, the major velocity discontinuities from Fig. 9 are shown as stippled lines west of 430 km while in the East the results from the depth converted (based on interval velocities adopted from stacking velocities) reflection seismic lines BGR98-01A, -01B are used. In the upper panel the dotted line shows the observed free-air anomaly and the continuous line our preferred final model anomaly. Between 300 and 460 km three alternatives are shown: The fine stippled line results when relatively uniform densities for the middle crust are used as shown in the cross-section. The continuous line fits the gravity maximum (Intrusion?) due to an increased density of 2.9 g cm^{-3} for the highlighted body (labelled (1) in the inset) in the middle crust. The coarse stippled line shows the resulting model curve if the density of a triangle shaped body at 400–450 km distance (labelled (2) in the inset) is reduced from 2.7 g cm^{-3} (igneous crust) to 2.55 g cm^{-3} (sediments). Albeit this curve fits the measured anomaly including the gravity minimum at 430 km offset nearly perfectly, we do not prefer this alternative. See text for explanation.

in graben structures beneath the BU (Fig. 5) . The syn-rift fill between the BU and the basement was modelled with a velocity of 5.0 to 5.2 km s^{-1}. Enlarged views of seismic sections with no gain applied (Figs 12 and 13) illustrate the crustal reflectivity. Zones of low reflection amplitudes in the MCS data coincide with higher crustal velocities (5.9 km s^{-1}) as derived from refraction modelling (Fig. 12, top). The most striking example is shown in Fig. 13. An about 20-km-wide lower crustal sector (indicated as intrusion in Fig. 13, lower panel) differs from the surrounding area not only in the reflection amplitudes but shows also a contrasting internal structuring. We found a velocity of at least 6.2 km s^{-1} for this structure that may indicate the presence of intrusives and/or extrusives that extend from the basement horizon down to the lower crustal layer or even deeper. The middle and lower crust show also an increase in the average velocity (6.5 km s^{-1} and 7.2 km s^{-1}, respectively) at this location and in addition a convex shape of both layers was necessary to obtain a reasonable fit with the data. Furthermore, there is a local maximum in the gravity anomaly around 370 km (Fig. 10, upper panel, labelled as 'Intrusion?'). A reasonable fit to this maximum cannot be obtained when only slightly varying densities in the middle crust, as shown in the lower panel of Fig. 10, are used. Therefore, we increased the density of a 40-km-wide body [labelled (1) in the inset box of Fig. 10] near the location of the gravity maximum to 2.9 g cm^{-3}. This body represents the proposed high-velocity intrusion and causes a nearly perfect fit to the observed gravity high. Albeit the western limit of the middle crustal body is displaced for about 10 km to the east in comparison with the high-velocity body as derived from refraction modelling the lower crustal high-density structures

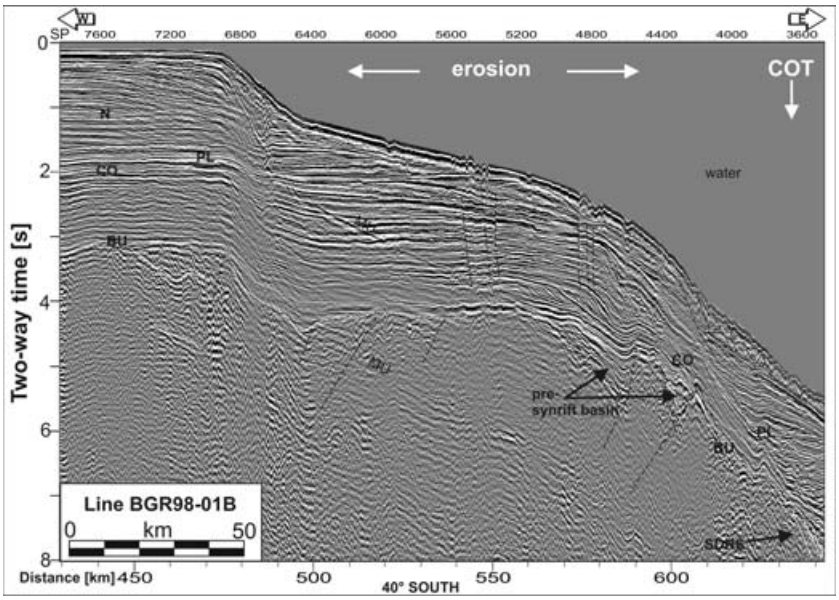

Figure 11. Interpreted reflection seismic section from migrated line BGR98-01B traversing the easternmost part of the Colorado Basin in E–W direction. The data are displayed with an AGC (1000 ms). The seismic marker horizons are indicated (for the nomenclature see Fig. 3). At the location of the seaward-dipping reflector sequences (SDRS) the continent–ocean transition (COT) was interpreted. For location of the line see Figs 2 and 10.

point also towards an interpretation of intrusives and/or extrusives in the deep part of the Colorado Basin.

Beside this location the middle crust was modelled with a velocity of 6.3 km s^{-1} and the lower crust shows a uniform velocity of 6.9 km s^{-1} in the western part of the line that increases to 7.2 km s^{-1} east of the distance 340 km. In the gravity model the basement shows densities increasing from 2.65 g cm^{-3} in the west to 2.7 g cm^{-3} in the east. To accomplish a reasonable fit with the measured values an increase in the density values for the middle and lower crust was necessary in the offset ranges between 170 and 390 km and between 100 and 430 km, respectively. In this offset range the offshore extension of the Ventana Hills is interpreted as illustrated in Fig. 9. It is proposed that the higher gravity values reflect this structural change.

While the main sedimentary unconformities and the top of the basement identified in the reflection seismic data fit quite well with the time converted refraction model boundaries (Figs 5 and 12) the correlation of middle to lower crustal layers with reflection patterns identified in the MCS data was only in part successful. Mid-crustal reflections predominate in the distance range from 50 to 250 km and show a convex structure with its shallowest point at approximately 180 km distance. These reflections are marked in Fig. 5 with arrows. The layer modelled with the refraction seismic data is up to 2 s (TWT) shallower but resembles the shape of the structure. To the east there are only rare reflections that might correlate with this layer. The same is true for the lower crustal layer. Indications for Moho reflections are present in the MCS data that correlate in the west with the refraction Moho but in the middle of the line there is a difference of 0.5 to 1 s (twt) between them. The Moho was modelled with a uniform velocity of 8.1 km s^{-1} and a uniform density of 3.33 g cm^{-3}.

The overall velocity structure of the refraction model fits quite well the extended primary crustal type as derived from refraction seismic data worldwide (Holbrook *et al.* 1992; Christensen & Mooney 1995). These authors report an average 6.0–6.3 km s^{-1} layer to a depth of ∼12 km followed by a 6.3 km s^{-1} layer that reaches to a depth of ∼22 km where another 10-km-thick layer shows a velocity of 6.6 km s^{-1}. The average Moho velocity for a rifted or extended continental crustal type is around 8.0 km s^{-1}.

In addition to the refraction model the gravity model (Fig. 10) comprises the passive margin imaged by the reflection seismic sections BGR98-01B (Fig. 11). For the continental part of the margin the densities of principal crustal units (sediments, upper, middle and lower crust) were extrapolated from the refraction model. The thickness and structure of the oceanic crust was adjusted to meet the long-wavelength behaviour of the gravity field. The only outstanding feature is a high-density structure (3.10 g cm^{-3}) in the lower crust below the continental rise/slope (at 650 km). It may correspond to the well-known high-velocity lower crustal structures that can be often observed at volcanic passive margins. This body that was incorporated in the model only to fit the measured gravity and without direct evidence from seismics indeed lies below the volcanic seaward-dipping reflector sequences (SDRS; Hinz *et al.* 1999) that were identified on this line (Fig. 11).

DISCUSSION

Basin structure

A decline in the Colorado Basin's sedimentary load resting on the BU east of approximately 304°E is obvious. This was established by Max *et al.* (1999) and others and is also clearly imaged in Fig. 2, where a band of blue colours separates the huge sedimentary infill of the Colorado Basin on the shelf from the deep-sea basin. However, this is mainly due to strong erosion of the uppermost sediments in a region where the steep slope reaches water depths exceeding 1500 m. Fig. 10 images the sedimentary and crustal structures from the onshore region across the entire shelf to the Argentine deep-sea basin. The BU is found in around 5 km depth (∼3 s (twt)) from the Colorado Basin to nearly the position of the interpreted continent–ocean transition (COT). An example seismic section (Fig. 11) illustrates the strong erosion affecting the Late Cretaceous to Tertiary

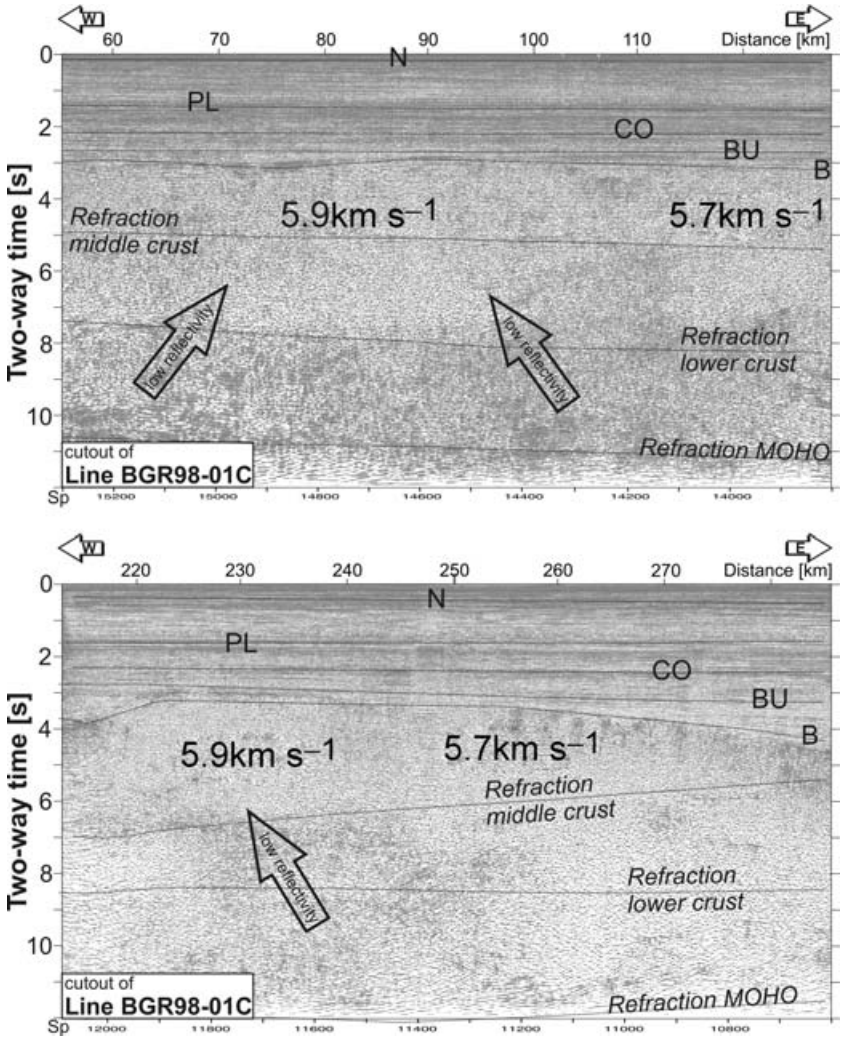

Figure 12. Example reflection seismic sections from line BGR98-01C. The data are displayed with no gain. Superimposed are the boundaries from the refraction seismic model converted to two-way traveltime. Nomenclature of the horizons is the same as in Fig. 3. The arrows mark locations of higher crustal velocities (5.9 km s^{-1}) resulting from refraction modelling that coincides with zones of slightly reduced reflectivity. For location of the section see Fig. 5.

sediments while the BU lies in the west of this line in a depth around 3 s (twt) and dips towards the east. There are several pre-/ and syn-rift grabens beneath the BU distributed along the line. Furthermore, variations in the depth of the BU in the range of ± 1.5 km occur. However, there are no indications for a 'basement high' as, for example, illustrated by Dingle *et al.* (1983) and frequently citied later (e.g. Maslanyj *et al.* 1992; Max *et al.* 1999; Bushnell *et al.* 2000), showing a bow-up of the basement of at least 2.5 km. We conclude that the smaller sedimentary load at the relatively steep slope is no argument against the idea that the Colorado Basin developed or, at least, was reactivated in combination with the early opening of the South Atlantic. A connection with the Orange Basin off South Africa in an initial stage of the basin evolution seems probable.

Evolution of the Colorado Basin

The observed E–W trend of the Colorado Basin, that is, perpendicular to the shelf, may be a product of either a strike-slip generated pull-apart basin, or the opening direction affecting the later South Atlantic region was initially NNW, towards the Macachin Graben onshore Argentina (Fig. 1). The latter is a linear belt of transtensional subsidence that runs from the Colorado Basin in NW direction and may be explained by rifting (Tankard *et al.* 1995). The Macachin Graben is thus in favour for the interpretation of the Colorado Basin as failed rift that developed in an early stage of the formation of the South Atlantic. The post-Upper Jurassic Colorado and Fortin Formation of mostly non-marine origin (Bushnell *et al.* 2000, see Fig. 3) and the presence of basaltic intrusions of Upper Jurassic/Lower Cretaceous age in the Salado Basin as well as the indications for a comparable intrusion in the Colorado Basin support the model of rift movements in both basins. The absence of a 'basement high' separating the Colorado Basin from the oceanic domain and clear indications for normal faults on both sides (north and south) of the basin are also in accordance with this assumption.

The duration of the extensional phase preceding the final break-up of the South Atlantic is unclear. Most authors suggest an extensional period of about 25 Ma (Uliana *et al.* 1989; Harry & Sawyer 1992) preceding the final break-up at around 130 Ma (Rabinowitz & LaBrecque 1979). Nürnberg & Müller (1991) proposed for a plate tectonic reconstruction a northward propagation of the South Atlantic rift from the southernmost tip of the South Atlantic to about 38°S in the vicinity of the Salado Basin from 150 to 130 Ma. In

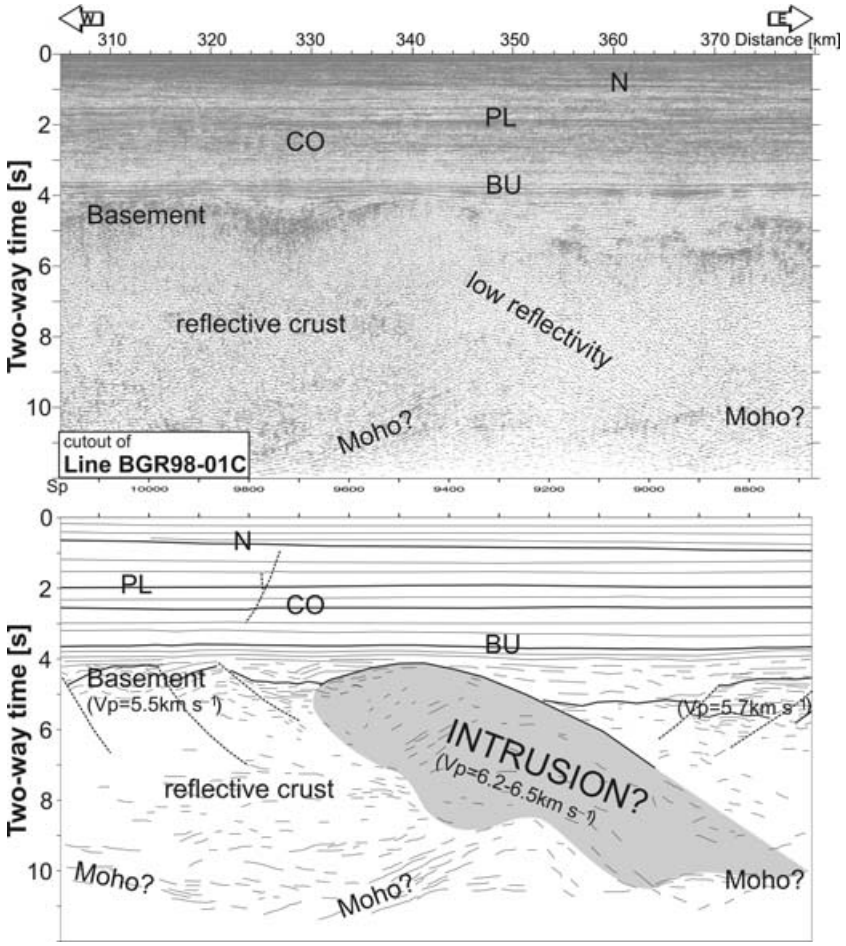

Figure 13. Example reflection seismic section from line BGR98-01C shown with no gain (top) and interpretation (bottom). Nomenclature of the horizons is the same as in Fig. 3. The highlighted area coincides with a zone of poor reflectivity in the MCS data and refraction modelling resulted in high velocities for both the upper and lower crust in this part. We tentatively interpret this structure as magmatic/volcanic intrusives/extrusives. For location of the section see Fig. 5.

this period continental stretching and minor dextral strike-slip motion was proposed within the Colorado and Salado Basins. If these basins developed within this 150 to 130 Ma period, extension must have changed the direction at the end of their formation, followed by the propagating opening of the South Atlantic in NE direction. The lower end time for the formation of the Colorado Basin may be estimated from deep-sea structures. The fact that the seaward-dipping reflector sequences (SDRS; *cf.* Fig. 11) run without a gap or separation along the Argentine slope (Hinz *et al.* 1999) defines the minimum age of the formation of the Colorado Basin. The emplacement of the SDRS (*cf.* Fig. 11) probably forming the magnetic anomaly G (Hinz *et al.* 1999) is supposed to be coincident with magnetic anomaly M10 or M11 (133–130 Ma), that is, the final formation of the Colorado Basin was before that time. Some minor tectonic (rift-related) activity, most probably in conjunction with the rift/drift phase of the South Atlantic, continued to affect the outer Colorado Basin into the latest Cretaceous. This is proven by the association of the flood basalts within the Pedro Luro sedimentary succession encountered in the Ranquel well (Kelley & Light 1993).

Basement composition

The basement of the Colorado Basin was found to be structurally heterogeneous. We propose that this heterogeneity is related the onshore geology. Urien *et al.* (1981) assumed the development of the Colorado Basin along a zone of weakening of the Late Palaeozoic (Permian–Early Triassic according to Uliana & Biddle 1987) Tandil (or Sierras Setenttrionales) and Ventana (or Sierras Australes) Hills. The latter probably represent the western continuation of the Cape Fold Belt in South Africa (e.g. Dingle *et al.* 1983; Uliana & Biddle 1987; Andreis *et al.* 1989; Kelley & Light 1993) and mark the transition from the stable Rio de la Plata craton in the north to the Patagonia terrane in the south (Ramos 1988, Urien *et al.* 1995; RdlP & PT in Fig. 1).

Assuming that the Ventana Hills (Fig. 2) represent the western continuation of the Cape Fold Belt in South Africa this structure must cross the Colorado Basin. A distinct velocity increase in the basement in an offset range from 120–220 km (Fig. 9) may represent the deeply buried continuation of this fold belt. In the MCS data a distinct bow-like structure in the deep crust [6–8 s (twt)] is visible at this location (Fig. 5; distance 100–250 km) and the top of this structure at a depth of ~3–3.5 s (twt; Fig. 5) shows an asymmetrically folded succession. A similar situation is reported for the Ventana Hills (Kelley & Light 1993). We interpret this part of line BGR98-01C (distance 120–220 km) as equivalents of the folded succession of the Ventana Hills of probably Permo–Carboniferous age. This interpretation is confirmed by the seismic image from Line BGR98-04 (Fig. 6). The northern part of the basin, which is in prolongation

of the supposed offshore extension of the Ventana Hills, is underlain by a series of asymmetric folds characterized by strong reflectivity, while the southern part shows a homogeneously layered basement.

A southeast wards offshore continuation of the inferred Claromecó depocentre beneath the Colorado Basin, as suggested by Keeley & Light (1993), seems also probable. Moreover the NW–SE orientation of the deep depocentre within the Colorado Basin (Fig. 2; 302°–304°E) fits with the projected continuation of the Claromecó depocentre and indicates such a link. The basement of the easternmost part of line BGR98-01C and of the adjacent line BGR98-01B is assumed to consist of Palaeozoic to Middle Mesozoic rocks of the Patagonia terrane (Urien & Zambrano 1996).

It appears plausible that magmatic intrusions concentrate where a maximum pre-weakening of the crust occurs. In the study area, the interpreted intrusion/extrusion at a distance of 350 km (Fig. 9) coincides with the deepest part of the pre-/synrift graben within the Colorado Basin. Such igneous bodies are probably linked to Upper Jurassic/Lower Cretaceous basalts that form injections into faults in the Salado Basin (Urien *et al.* 1976) and volcanics encountered at the deepest part of the well Cruz del Sur of the same age.

SUMMARY AND CONCLUSIONS

The presented data indicate that the Colorado Basin probably is a typical extensional basin and not an intracontinental sag basin. The origin of the oblique rift most probably resulted from extensional stress, acting either through or interfering with the prevailing Palaeozoic basement fabric, oriented NW–SE. The basin developed across the suggested offshore extension of the buried Ventana Hills at the transition from the stable Rio de la Plata craton in the north to the Patagonia terrane in the south (Ramos 1988; Urien *et al.* 1995). The zone of weakening that finally gave the space for the basin may be related to earlier backarc extension that resulted in the development of several basins at the southwestern margin of the Rio del la Plata craton. At the proposed intersection of the Colorado Basin with the offshore extension of the Claromecó depocentre the maximum thickness of pre-/and synrift infill was found. A strike-slip component in the basins evolution can not be ruled out and it thus may be interpreted as pull-apart basin. However, we suggest that the Colorado Basin represents a failed rift structure for the following reasons: The basin probably was affected by magmatic/volcanic intrusives/extrusives associated with the opening of the South Atlantic. The basin's floor is more or less flat across the shelf. It shows a gentle rise at the shelf break and deepens towards the deep-sea basin where it finally merges with the seaward-dipping reflector sequences. Lines running perpendicular to the basins axis show extensional faults.

The modelling results are in favour of a continuation of the main onshore geological features beneath the sedimentary infill of the Colorado Basin. We interpret the basement along the line BGR98-01C from west to east as offshore continuation of the Ventana Hills, the Claromecó depocentre, and of Palaeozoic to Middle Mesozoic rocks of the Patagonia terrane. In the deepest part of the pre-/synrift graben within the Colorado Basin a volcanic/igneous intrusion was interpreted forming a dike/sill feature along an extensional fault. We suggest that these supposed basalts are of the same age as the Upper Jurassic/Lower Cretaceous basalts that form intrusions in the Salado Basin (Urien *et al.* 1976).

ACKNOWLEDGMENTS

For fruitful discussions and insights into industrial data we are grateful to Antonio Nevistic and Oscar Mancilla from REPSOL/YPF, Argentina. We are grateful to Karl Hinz for continuous assistance, motivation and scientific advice. We would like to thank W. Jokat from the Alfred Wegener Institute (AWI), Germany for the possibility to use five of their OBH systems. Journal reviews by two anonymous reviewers are gratefully acknowledged. Funding of the BGR98 seismic survey and this work was provided by the Federal Institute for Geosciences and Natural Resources (BGR), Hannover, Germany.

REFERENCES

Andreis, R.R., Iniguez, L.L., Lluch, L.L. & Rodriguez, R., 1989. Cuenca Paleozoica de Ventania, Sierras Australes, Provincia de buenos Aires, *in Cuencas sedimentarias Argentinas (Serie Correlacion 6)*, pp. 265–298, eds Chebli, G. & Spalletti, L., Universidad Nacional de Tucumen, Argentina.

Bushnell, D.C., Baldi, J.E., Bettini, F.H., Franzin, H., Kovas, E., Marinelli, R. & Wartenburg, G.J., 2000. Petroleum system analysis of the Eastern Colorado Basin, offshore Northern Argentine, in *Petroleum systems of South Atlantic margins*, pp. 403–415, ed. Mello, M.R., Am. Assoc. Petrol. Geol. Mem., 29, USA.

Christensen, N.I. & Mooney, W.D., 1995. Seismic velocity structure and composition of the continental crust; a global view, *J. geophys. Res.*, **100**(6), 9761–9788.

Dalziel, I.W.D., Storey, B.C., Garret, S.W., Grunow, A.M., Herrod, L.D.B. & Pankhurst, R.J., 1987. Extensional tectonics and the fragmentation of Gondwanaland, in *Continental Extension Tectonics*, pp. 433–441, eds Dewey, J.F. and Hancock, P.L., Spec. Publ. Geol. Soc. London, 28, London.

Dingle, R.V., Siesser, W.G. & Newton, A.R., 1983. *Mesozoic and Tertiary geology of Southern Africa*, A.A. Balkema, Rotterdam, p. 375.

Flueh, E.R. & Bialas, J., 1996. A digital, high data capacity ocean bottom recorder for seismic investigations, *Int. Underwater Syst. Design,* **18,** 18–20.

Fryklund, B., Marshal, A. & Stevens, J., 1996. Cuenca del Colorado, in *Geologia y recursos naturales de la plataforma continental Argentina, relatario XIII° Congreso Geologico Argentino y III° Congreso de Exploracion de Hidrocarboros*, pp. 135–158, eds Ramos, V.A. & Turic, M.A., Association Geologica Argentina & Inst. Argentino del Petroleo, Buenos Aires, Argentina.

Harry, D.L. & Sawyer, D.S., 1992. Basaltic volcanism, mantle plumes and the mechanics of rifting: the Parana flood basalt province of South America, *Geology,* **20,** 207–210.

Hinz, K., Neben, S., Schreckenberger, B., Roeser, H.A., Block, M., Gonzalvez de Souza, K. & Meyer, H., 1999. The Argentine continental Margin north of 48° S: Sedimentary successions, volcanic activity during breakup. *Mar. Petrol. Geol.,* **16,** 1–25.

Holbrook, W.S., Mooney, W.D. & Christensen, N.I., 1992. The seismic velocity structure of the deep continental crust, in *Continental Lower Crust, Developments in Geotectonics*, Vol. 23, pp. 1–43, eds Fountain, D.M. Arculuc, R. & Kay, R.W., Elsevier, Amsterdam, The Netherlands.

Iniguez, A.M., Del Valle, A., Poire, D.G., Spalletti, L.A. & Zalba, P.E., 1989. Cuenca PreCambria/Paleozoica Inferior de Tandilia, Provincia de Buenos Aires, in *Cuencas sedimentarias Argentinas (Serie Correlacion 6)*, pp. 245–263, eds Chebli, G. & Spalletti, L., Universidad Nacional de Tucumen, Argentina.

Juan, R. del C., De Jager, J., Russell, J. & Gebhard, I., 1996. Flanco norte de la cuenca del Colorado, in Geologia y recursos naturales de la plataforma continental Argentina, relatario XIII° Congreso Geologico Argentino y III° Congreso de Exploracion de Hidrocarboros, pp. 117–134, eds Ramos, V.A. & Turic, M.A., Association Geologica Argentina & Inst. Argentino del Petroleo, Buenos Aires, Argentina.

Kaasschieter, J., 1963. Geology of the Colorado Basin, *Tulsa Geological Society Digest,* **31,** 177–187.

Kaasschieter, J., 1965. Geologia de la Cuenca del Colorado, *Acta Geologica Lilloana,* **7**(3), 251–269.

Keeley, M.L. & Light, M.P.R., 1993. Basin evolution and prospectiveity of the Argentine continental margin, *Journal of Petroleum Geology,* **16**(4), 451–464.

LaCoste, L.J.B., 1973. Cross correlation method for evaluating and correcting shipboard gravity data, *Geophysics,* **38**(4), 701–709.

Lawver, L.A., Gahagan, L.M. & Dalziel, I.W.D., 1998. A tight fit – Early Mesozoic Gondwana, a plate reconstruction perspective, *Mem. Natl. Inst. Polar. Res., Spec. Issue,* **53,** 214–229.

Lesta, P.J., Turic, M.A. & Mainardi, E., 1978. Actualization de la information estratigrafica en la Cuenca del Colorado, *VII° Congresso Geologico Argentino (Neuquen, 1978)*, Actas I, pp. 701–713, Buenos Aires.

Light, M.P.R., Keeley, M.L., Maslanyi, M.P. & Urien, C.M., 1993. The tectono-stratigraphic development of Patagonia, and its relevance to hydrocarbon exploration, *Journal of Petroleum Geology,* **16**(4), 465–482.

Ludwig, W., Nafe, J. & Drake, C., 1970. Seismic refraction, in *The Sea*, Vol. 4, ed. Maxwell, A., Wiley-Interscience.

Ludwig, W.J., Ewing, J.I., Windish, C.C., Lonardi, A.g. & Rios, F.F., 1979. Structure of the Colorado Basin and continent ocean crust boundary off Bahia Blanca, Argentina, in *Geological and Geophysical Investigations of Continental Margins*, pp. 113–124, eds Watkins, J.S., Montadert, L. & Wood, P., Am. Assoc. Petrol. Geol. Mem., 29, Tulsa, USA.

Maslanyj, M.P., Light, M.P.R., Greenwood, R.J. & Banks, N.L., 1992. Extension tectonics offshore Namibia and evidence for passive rifting in the South Atlantic, *Marine and Petroleum Geology,* **9,** 590–601.

Max, M.D., Ghidella, H., Kovacs, L., Paterlini, M. & Valladares, J.A., 1999. Geology of the Argentine continental shelf and margin from aeromagnetic survey, *Marine and Petroleum Geology,* **16,** 41–64.

Nürnberg, D. & Müller, R.D., 1991. The tectonic evolution of the South Atlantic from Late Jurassic to present *Tectonophysics,* **191,** 27–53.

Rabinowitz, P.D. & LaBrecque, J., 1979. The Mesozoic South Atlantic Ocean and evolution of its continental margins, *J. geophys. Res.,* **84,** 5.973–6.002.

Ramos, V.A., 1988. Late Proterozoic-early Paleozoic of South America—a collisional history, *Episodes,* **11**(3), 168–188.

Ramos, V.A. & Turic, M.A., 1996. Geologia y Recursos Naturales de la Plataforma Continental Argentina, *Asociacion Geol. Arg. e Inst. Arg. Petr.*, pp. 452, Buenos Aires.

Tankard, A.J., Jackson, M.P.A., Erickson, K.A., Hobday, D.K., Hunter, D.R. & Minter, W.E.C., 1982. in *Crustal Evolution of Southern Africa, 3.8 Billion Years of Earth History*, p. 502, Springer, New York.

Tankard, A.J. et al., 1995. Structural and Tectonic Controls of Basin Evolution in Southwestern Gondwana During the Phenerozoic, in *Petroleum Basins of South America*, pp. 5–52, eds Tankard, A.J., Suárez Soruco, R. & Welsink, H.J., Am. Assoc. Petrol. Geol. Mem., 62, USA.

Turic, M.E. & Diaz, H., 1987. Cuencas del Salado y del Colorado, *Actas DelDecimo Congreso Geologico Argentino*, 29–32.

Uliana, M.A. & Biddle, K.T., 1987. Permian to Late Cenozoic evolution of Patagonia, main tectonic events, magmatic activity, and depositional trends, in *Gondwana six: structure, tectonics, and geophysics, Am. Geophys. Monograph, 40*, pp. 271–286, ed. McKenzie, G.D., AGU, Washington, DC.

Uliana, M.A., Biddle, K.T. & Cerdan, J., 1989. Mesozoic extension and the formation of Argentine sedimentary basins, in *Extensional tectonics and stratigraphy of the North Atlantic margins*, pp. 599–614, eds Tankard, A.J. & Balkwill, H.R., Am. Assoc. Petrol. Geol. Mem., 46, USA.

Unternehr, P., Curie, D., Olivet, J., Goslin, J. & Beuzart, P., 1988. South Atlantic fits and intraplate boundaries in Africa and South America, *Tectonophysics,* **155,** 169–179.

Urien, C.M. & Zambrano, J.J., 1973. The geology of the basins of the Argentine continental margin and Malvinas Plateau, in *The Ocean Basins and Margins*, pp. 135–169, eds Nairn, A.E.M. & Stehli, F.G., Plenum Press, New York.

Urien, C.M., Martins, L.R. & Zambrano, J.J., 1976. The geology and tectonic framework of southern Brazil, Uruguay and North Argentina continental margin; their behavior during the Southern Atlantic opening, in *Continental Margins of the Atlantic Type, Anais da Academia Brasileira de Ciencias*, Vol. 48, pp. 365–376, Sao Paulo.

Urien, C.M., Zambrano, J.J. & Martins, L.R., 1981. The basins of southeastern South America (southern Brazil, Uruguay, and eastern Argentina), including the Malvinas Plateau and southern South Atlantic paleogeographic evolution, in *Cuencas sedimentarias del Jurasico y Cretacico en America del Sur: Comite Sudamericano del Jurasico y Cretacico*, Vol. 1, pp. 45–126, eds Volkheimer, W. & Musacchio, E.A.

Urien, C.M., Zambrano, J.J. & Yrigoyen, M.R., 1995. Petroleum basins of southern South America: an overview, in *Petroleum basins of South America*, pp. 63–77, eds Tankard, A.J. Suárez Soruco, R. & Welsink, H.J., Am. Assoc. Petrol. Geol. Mem., 62, USA.

Urien, C.M. & Zambrano, J.J., 1996. Estructura del Margen Continental, in *Geologia y recursos naturales de la plataforma continental Argentina, relatario XIII° Congreso Geologico Argentino y III° Congreso de Exploracion de Hidrocarboros*, pp. 29–66, eds Ramos, V.A. & Turic, M.A., Association Geologica Argentina & Inst. Argentino del Petroleo, Buenos Aires, Argentina.

Zelt, C.A. & Smith, R.B., 1992. Seismic traveltime inversion for 2-D crustal velocity structure, *Geophys. J. Int.,* **108,** 16–34.

Zelt, C.A., 1999. Modelling strategies and model assessment for wide-angle seismic traveltime data, *Geophys. J. Int.,* **139,** 183–204.